

# Zr<sub>1-x</sub>Ln<sub>x</sub>W<sub>2</sub>O<sub>8-x/2</sub> (Ln = Eu, Er, Yb): Solid solutions of negative thermal expansion-synthesis, characterization and limited solid solubility

Hai-Hua Li<sup>a</sup>, Jing-Sa Han<sup>a</sup>, Hui Ma<sup>b</sup>, Ling Huang<sup>a</sup>, Xin-Hua Zhao<sup>a,\*</sup>

<sup>a</sup>Department of Chemistry, Beijing Normal University, Beijing 100875, PR China

<sup>b</sup>Analysis and Test Center, Beijing Normal University, Beijing 100875, PR China

Received 18 September 2006; received in revised form 28 November 2006; accepted 4 December 2006

Available online 15 December 2006

## Abstract

Zr<sub>1-x</sub>Ln<sub>x</sub>W<sub>2</sub>O<sub>8-x/2</sub> solid solutions (Ln = Eu, Er, Yb) of different substitution fractions  $x$  have been synthesized. Their X-ray diffraction (XRD) patterns have been indexed and lattice parameters calculated based on the  $\alpha$ -ZrW<sub>2</sub>O<sub>8</sub> structure. The coefficients of thermal expansion (CTEs) of these solid solutions were estimated to be  $-10.3 \times 10^{-6} \text{ K}^{-1}$  in temperature range of 30–100 °C. The solubility of lanthanide ions in these solid solutions decreases linearly with the increase in the radius of substituted lanthanide ions. Based on the concentration dependence of phase transition temperatures, a novel method for determination of solubility of the lanthanide ions in Zr<sub>1-x</sub>Ln<sub>x</sub>W<sub>2</sub>O<sub>8-x/2</sub> solid solutions has been developed. This method seems to be more sensitive as compared with that based on XRD technique.

© 2006 Elsevier Inc. All rights reserved.

**Keywords:** Solid solution; Solid solubility; Negative thermal expansion; Zr<sub>1-x</sub>Ln<sub>x</sub>W<sub>2</sub>O<sub>8-x/2</sub>

## 1. Introduction

Substantial interest of both scientists and engineers has been directed towards the cubic ZrW<sub>2</sub>O<sub>8</sub>-type compounds due to their isotropic negative thermal expansion (NTE) property over a wide temperature range (from 272.9 to 777 °C and 1107 to 1257 °C, respectively) [1–4]. Special efforts in recent years have been devoted to improve their thermal as well as mechanical performance through the study of ZrW<sub>2-x</sub>Mo<sub>x</sub>O<sub>8</sub> solid solutions [5–12]. Similar effects have been observed upon substitution of Zr<sup>4+</sup> by lower valent cations such as Sc<sup>3+</sup>, Y<sup>3+</sup>, In<sup>3+</sup> and Lu<sup>3+</sup>, [13,14] despite the fact that the solid solubility of these doping ions is limited.

In this paper, we report synthesis and DSC, X-ray diffraction (XRD)-characterization of a series of solid solutions with cubic ZrW<sub>2</sub>O<sub>8</sub> structure, in which the crystal sites of Zr<sup>4+</sup> are substituted partially by lanthanide cations

Ln<sup>3+</sup> (Ln = Yb, Er and Eu). It has been found that the solubility of lanthanide cations in Zr<sub>1-x</sub>Ln<sub>x</sub>W<sub>2</sub>O<sub>8-x/2</sub> solid solutions increases as the radius of the lanthanide cation decreases. In the meantime, an approach to determine the solubility limit of sparingly soluble Ln<sup>3+</sup> ions has been developed.

## 2. Experimental section

The raw materials ZrO(NO<sub>3</sub>)<sub>2</sub> · 2H<sub>2</sub>O, Yb<sub>2</sub>O<sub>3</sub> (99.99%), Er<sub>2</sub>O<sub>3</sub> (99.99%) and 5(NH<sub>4</sub>)<sub>2</sub> · 12WO<sub>3</sub> · 5H<sub>2</sub>O used for samples preparation were commercially available reagents from Beijing Chemical Reagents Company and Tianjin Juneng Chemical Company Ltd., respectively. The numbers of hydrated water in the raw materials have been checked through gravimetric determination. The samples were prepared by dropwise addition of [(1-x') Zr<sup>4+</sup> + x' Ln<sup>3+</sup>] aqueous mixture of assigned ionic concentration  $x'$  into the aqueous slurry consisted of given amount of W (VI) in deionized water. The white powder obtained by drying the reactant mixture at 100 °C was then annealed at

\*Corresponding author. Fax: +86 10 6220 7971.

E-mail address: [xinhauz@bnu.edu.cn](mailto:xinhauz@bnu.edu.cn) (X.-H. Zhao).

600 °C for 3 h, and used as the precursors of the  $Zr_{1-x}Ln_xW_2O_{8-x/2}$  solid solutions. After grinding, pressing, the precursor pellet was sintered at high temperature for 5 h according to the heating condition listed in Table 1 and then quenched in ambient atmosphere immediately.

Both DSC and XRD measurements were carried out by routine procedure described previously [11]. Briefly, room temperature and variable temperature XRD data were collected from 10° to 100° (2 $\theta$ ) in ambient atmosphere on a Philips X'-Pert MPD diffractometer and a TCU 2000 unit is equipped to control the temperature in temperature-variable measurements.

The lattice parameters of cubic  $Zr_{1-x}Ln_xW_2O_{8-x/2}$  at different temperatures were deduced using Unitcell program [15] from the variable temperature XRD data. The XRD data calibrated with SiO<sub>2</sub> (JCPDS-PDF: 33-1161, Quartz) as internal standard were used to calculate the lattice parameters of cubic  $Zr_{1-x}Ln_xW_2O_{8-x/2}$  at room temperature. The sample used in measurements has been dehydrated completely, so the possible effect of trace water contained in sample was eliminated [3].

DSC curves in temperature range of 30–1300 °C were measured with heating rate of 10 °C/min on DTA-404 PC instrument (Netzsch) under air-atmosphere and an empty Pt crucible was used as the reference.

### 3. Results and discussion

#### 3.1. Synthesis and thermal analysis of $Zr_{1-x}Ln_xW_2O_{8-x/2}$ solid solutions

The preparation conditions for  $Zr_{1-x}Ln_xW_2O_{8-x/2}$  solid solutions ( $Ln = Yb, Er$  and  $Eu$ ) of different substitution fractions  $x$  were selected based on their DSC patterns combining with XRD measurement. Typical DSC-curves of  $Zr_{1-x}Yb_xW_2O_{8-x/2}$  solid solutions with  $x = 0, 0.01, 0.02, 0.03, 0.04$  are displayed in Fig. 1, which indicates that all solid solutions show a similar DSC pattern characterized by a single exothermic peak and two endothermic peaks, regardless of their lanthanide substitution fraction  $x$ . Considering the phase diagram of the  $ZrO_2$ – $WO_3$  system reported previously [16], the endothermic peak near 1258 °C can be assigned to the melting point of  $ZrW_2O_8$

and the appearance of the exothermic peak near 860 °C is most likely associated with the decomposition process of  $ZrW_2O_8$  into the binary oxides  $ZrO_2$  and  $WO_3$ .

A close inspection of these XRD patterns in Fig. 2 reveals that at 1120 °C only the peaks corresponding to  $WO_3$  (JCPDS-PDF: 83-0951) and  $ZrO_2$  (JCPDS-PDF: 86-1451) occur, but a weak reflection peak at 21° (2 $\theta$ ) appears at 1130 °C and it approaches to saturation at 1150 °C. This diffraction peak growing with temperature seems to be most likely associated with 210 reflection of cubic- $Zr_{0.96}Yb_{0.04}W_2O_{7.98}$  (as arrow shown). Hence, it is reasonable to assign the DSC endothermic peaks at 1128–1145 °C to the reaction responsible for cubic- $Zr_{1-x}Ln_xW_2O_{8-x/2}$  formation from its parent oxides. Therefore, the temperature between the two endothermic peaks can be selected as the reaction temperature (see Table 1).

#### 3.2. Lattice parameters and thermal expansion characteristics of $Yb, Er, and Eu$ -substituted solid solutions

The XRD patterns of the  $Zr_{1-x}Ln_xW_2O_{8-x/2}$  with  $Ln = Yb, Er$  and  $Eu$  at room temperature are presented in Fig. 3.

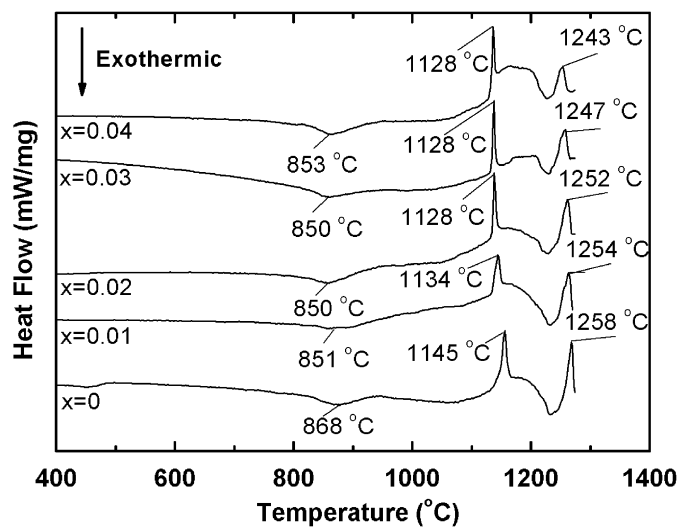


Fig. 1. DSC curves of  $Zr_{1-x}Yb_xW_2O_{8-x/2}$  solid solutions ( $x = 0, 0.01, 0.02, 0.03, 0.04$ ).

Table 1  
Heating conditions for preparing the solid solutions

The component of Yb (mol%)	Optimal heating system	The component of Er (mol%)	Optimal heating system	The component of Eu (mol%)	Optimal heating system
0	1200 °C 2 h and then 1160 °C 3 h	0	1200 °C 2 h and then 1160 °C 3 h	0	1200 °C 2 h and then 1160 °C 3 h
1	1200 °C 1 h and then 1160 °C 4 h	1	1200 °C 1 h and then 1160 °C 4 h	1	1200 °C 2 h and then 1160 °C 3 h
2, 3	1180 °C 1 h and then 1150 °C 4 h	2	1180 °C 1 h and then 1155 °C 4 h	2, 3	1200 °C 2 h and then 1160 °C 3 h
4, 5, 6, 8	1170 °C 1 h and then 1150 °C 4 h	3, 4, 5, 6	1170 °C 1 h and then 1155 °C 4 h	—	—

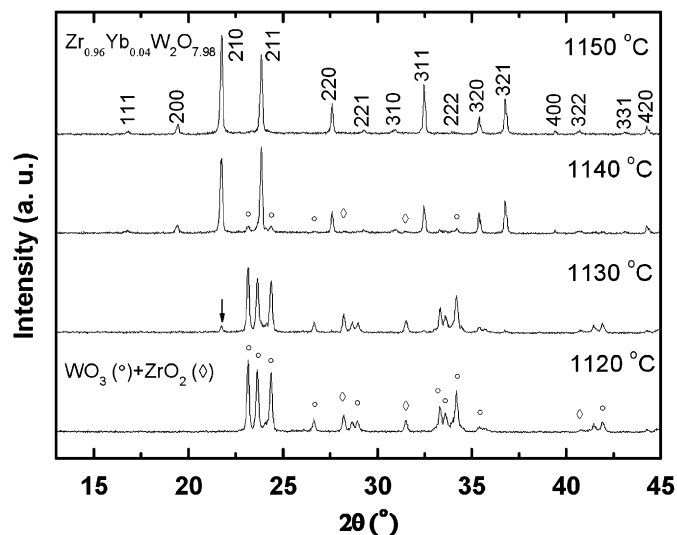


Fig. 2. XRD patterns of  $Zr_{0.96}Yb_{0.04}W_2O_{7.98}$  solid solution at different temperatures.

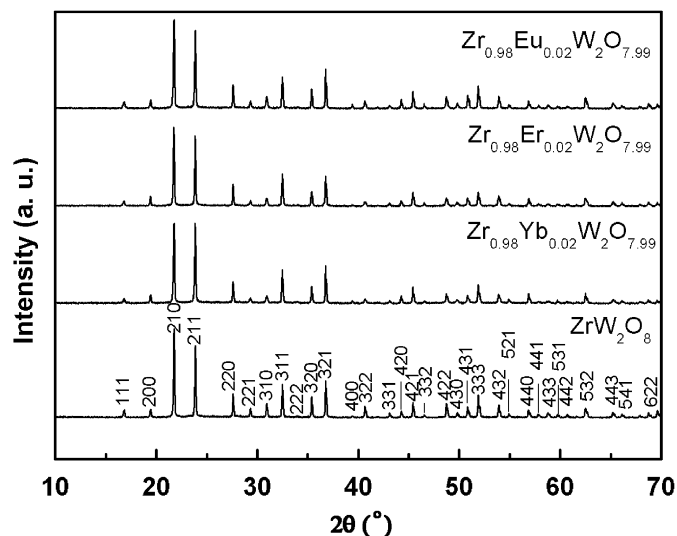


Fig. 3. XRD patterns of  $ZrW_2O_8$  and  $Zr_{0.98}Ln_{0.02}W_2O_{7.99}$  ( $Ln = Yb, Er, Eu$ ) at room temperature.

It can be seen that all solid solutions studied show the similar XRD patterns. We can index these XRD patterns using PowderX software [17] with a cubic unit cell corresponding to the  $ZrW_2O_8$  crystal structure. As we know the polymorphs of cubic  $ZrW_2O_8$  transforms from the order form (denoted  $\alpha$ - $ZrW_2O_8$  with space group:  $P2_13$ ) to the disorder form (denoted  $\beta$ - $ZrW_2O_8$  with space group:  $Pa\bar{3}$ ) at 428 K [2]. Therefore, according to the reflection conditions, the presence of reflection 310 enables us to identify these solid solutions as adopting the ordered  $\alpha$ - $ZrW_2O_8$  structure.

The dependence of the lattice parameters on  $Ln^{3+}$  ionic concentration  $x'$  in aqueous mixture is displayed in Fig. 4, which indicates clearly that the lattice parameters of  $Zr_{1-x}Ln_xW_2O_{8-x/2}$  solid solutions decrease linearly with increasing  $x'$  as predicted by Vegard's rule, but the

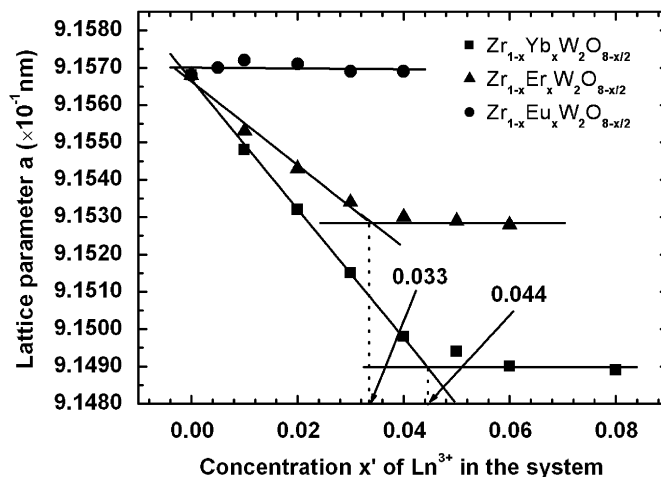


Fig. 4. Dependence of lattice parameters of  $Zr_{1-x}Ln_xW_2O_{8-x/2}$  on the concentration  $x'$  of  $Ln^{3+}$  in the system at 25 °C.

lattice parameters become invariant above a “threshold”  $x_{th}$ : specifically  $x_{th} \geq 0.044$  for  $Zr_{1-x}Yb_xW_2O_{8-x/2}$  and  $x_{th} \geq 0.033$  for  $Zr_{1-x}Er_xW_2O_{8-x/2}$ . Undoubtedly, the “threshold” is associated with a partial solubility of the lanthanide ion and the relationship between the lattice parameter and the concentration  $x$  of  $Ln^{3+}$  in the solid solutions can be described by following equations:

$$\text{For } Zr_{1-x}Yb_xW_2O_{8-x/2}, a = 9.1567 - 0.173x, \\ 0 < x \leq 0.044; R: 0.9994, SD: 1.1402 \times 10^{-4}. \quad (1)$$

$$\text{For } Zr_{1-x}Er_xW_2O_{8-x/2}, a = 9.1564 - 0.112x, \\ 0 < x \leq 0.033; R: 0.9923, SD: 2.2134 \times 10^{-4}. \quad (2)$$

It should be noted, however, that the “threshold”  $x_{th}$  of  $Zr_{1-x}Eu_xW_2O_{8-x/2}$  is a relative low value, which is difficult to be measured with sufficient accuracy by the traditional method based on XRD.

The lattice parameters evaluated for  $Zr_{1-x}Ln_xW_2O_{8-x/2}$  solid solutions studied at different temperatures, like their parent  $ZrW_2O_8$ , show clearly the NTE property, i.e., their average coefficient of thermal expansion (CTE) ( $\alpha = (a_T - a_{T_0}) / (a_{T_0}(T - T_0))$ ) evaluated from the slope of lattice parameter-temperature plots exhibits a invariant CTE of approximately  $-10.3 \times 10^{-6} K^{-1}$  in temperature range of 30–100 °C, but it decreases to a limited value about  $-5.1 \times 10^{-6} K^{-1}$  at temperature above 150 °C. The behaviors of  $Zr_{1-x}Yb_xW_2O_{8-x/2}$  presented in Fig. 5 services as a typical sample. Of interest to note that the slope of lattice parameters-temperature plots at temperature below  $\sim 100$  °C is almost the same for all  $Zr_{1-x}Ln_xW_2O_{8-x/2}$  solid solutions studied, but above this temperature a slope change is detected upon increasing temperature. Moreover, the plots for all  $Zr_{1-x}Ln_xW_2O_{8-x/2}$  solid solutions studied converge together in spite of differences in the nature and the concentrations of the lanthanide ions involved.

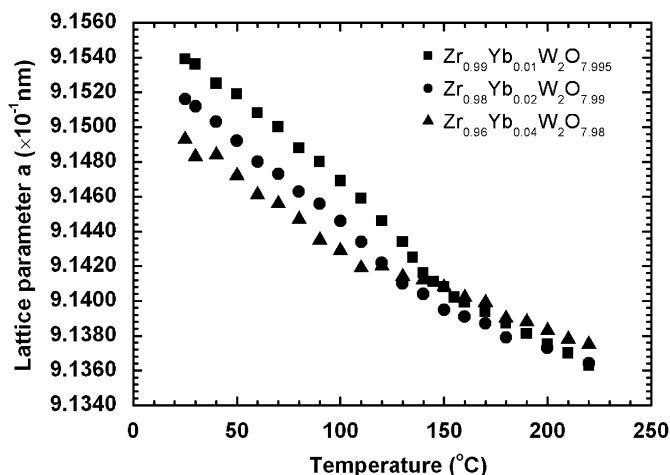


Fig. 5. Temperature dependence of lattice parameters of  $Zr_{1-x}Yb_xW_2O_{8-x/2}$  solid solutions.

### 3.3. Relative order degree parameter, phase transition temperature and solid solubility

For cubic  $ZrW_2O_8$ , the order–disorder phase transition is thought to be related with the orientation of  $WO_4$  groups. [2] To quantitatively describe this order–disorder phase transition in  $Zr_{1-x}Ln_xW_2O_{8-x/2}$  solid solutions, we introduce a characteristic parameter:  $\eta_T'$ , which corresponds to the degree of order in the  $WO_4$  orientations at a given temperature  $T$ , which, following Yamamura et al. [18] can be determined from the integrated intensity of reflection 310 normalized by that of fundamental reflection 210,  $I_{310}/I_{210}$ :

$$\eta_T' = \sqrt{\frac{[(I_{310}/I_{210})_{Zr_{1-x}M_xW_2O_{8-x/2}}]_T}{[(I_{310}/I_{210})_{ZrW_2O_8}]_{298K}}}$$

The relative order parameter,  $\eta_T'$  for  $Zr_{1-x}Ln_xW_2O_{8-x/2}$  ( $x = 0, 0.01, 0.02, 0.03, 0.04$  for  $Yb^{3+}$ ;  $x = 0.01, 0.02, 0.03$  for  $Er^{3+}$  and  $x = 0.005, 0.01, 0.02, 0.03$  for  $Eu$ ) were calculated from the refined integrated peak intensity using Philips Profile Fitting program, [19] and their values as a function of temperature  $T$  are displayed in Fig. 6. It is evident that  $\eta_T'$  decrease upon increasing temperature.

We define the temperature, at which  $\eta_T'$  approaches to zero, as the phase transition temperature,  $T_c$ . This characteristic temperature can be deduced simply by extrapolating  $\eta_T' \sim T$  curves to  $\eta_T' = 0$ . It can be seen in Fig. 7 that the phase transition temperatures,  $T_c$ 's obtained in this way are sensitive to changes in both the nature and doping level  $x$  of the  $Ln^{3+}$  ions. Interestingly, a remarkable decrease in  $T_c$  is observed for  $x$  values below 1.6 mol% in  $Zr_{1-x}Eu_xW_2O_{8-x/2}$  (see Fig. 7), above which a further increase in doping level  $x$  leads the  $T_c \sim x$  plot to level off indicating the solid solubility limit has been reached. The linear relations between  $T_c$ 's and concentration  $x$  of  $Ln^{3+}$  can be described quantitatively by equations:

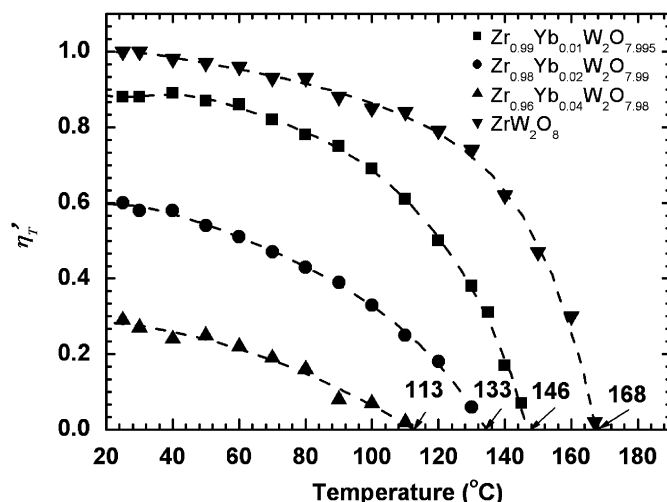


Fig. 6. Dependence of the relative order parameter  $\eta_T'$  on the temperature in  $Zr_{1-x}Ln_xW_2O_{8-x/2}$ . The phase transition temperature ( $T_c$ ) was determined by extrapolating  $\eta_T' \sim T$  curve to  $\eta_T' = 0$ .

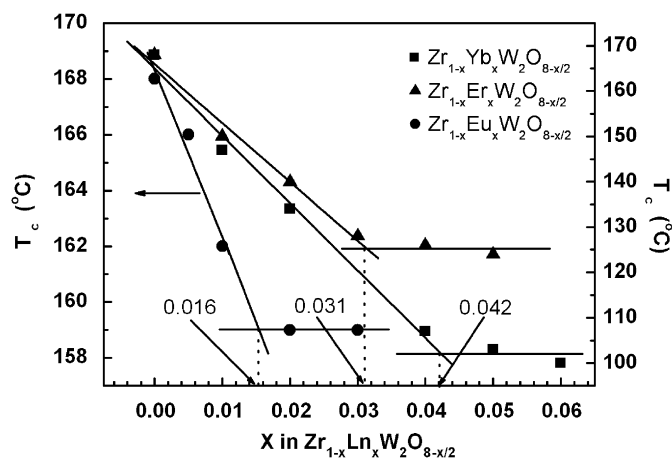


Fig. 7. Phase transition temperature ( $T_c$ ) of  $Zr_{1-x}Ln_xW_2O_{8-x/2}$  against the concentration ( $x$ ) of  $Ln^{3+}$ .

$$\text{For } Zr_{1-x}Yb_xW_2O_{8-x/2}, T_c(^{\circ}C) = 165.0 - 1485.7x, \\ 0 < x \leq 0.042; R : 0.9942, SD : 3.3594, \quad (3)$$

$$\text{For } Zr_{1-x}Er_xW_2O_{8-x/2}, T_c(^{\circ}C) = 166.0 - 1300x, \\ 0 < x \leq 0.031; R : 0.9918, SD : 2.6458, \quad (4)$$

$$\text{For } Zr_{1-x}Eu_xW_2O_{8-x/2}, T_c(^{\circ}C) = 168.3 - 600x, \\ 0 < x \leq 0.016; R : 0.9820, SD : 0.8165. \quad (5)$$

For  $Zr_{1-x}Ln_xW_2O_{8-x/2}$  ( $Ln = Yb, Er$ ), the solubility limits determined by  $T_c \sim x$  plots are in good agreement with those determined from lattice parameter,  $a \sim x$  plots. Therefore, it can be deduced that  $T_c$  may be used as an additional parameter, which affords increased sensitivity to ascertain the composition of solid solutions, especially for those ions with very limited solubility.

The limited solid solubility for selected partial solid solutions of  $Zr_{1-x}Ln_xW_2O_{8-x/2}$  as a function of the radii of corresponding lanthanide ions is displayed in Fig. 8. This

correlation demonstrates that the increase in solid solubility follows the lanthanide contraction trend in a way that is opposite to that observed for lattice parameter, i.e., the  $Zr_{1-x}Ln_xW_2O_{8-x/2}$  solid solutions containing smaller lanthanide ions exhibit a less pronounced lattice parameter contraction, but shows a higher limited solid solubility. Similar trends have been reported also for  $Zr_{1-x}M_xW_2O_{8-x/2}$  solid solutions with other metal ions  $M = Sc^{3+}$ ,  $In^{3+}$ ,  $Y^{3+}$  and  $Lu^{3+}$  [13,14]. This behavior seems to be understandable in terms of substitution-induced distortion of the local environment around W–O site due to charge compensation upon replacing  $Zr^{4+}$  by a trivalent lanthanide ion [18].

Finally, it should be noted that the relative order parameters at 25 °C,  $\eta_{25^\circ C}$  of  $Zr_{1-x}Ln_xW_2O_{8-x/2}$  solid solutions also decrease linearly with the increase in substitution fraction  $x$  (Fig. 9) as that observed for phase transition temperature  $T_c$  (Fig. 7). The similar  $x$ -dependence observed

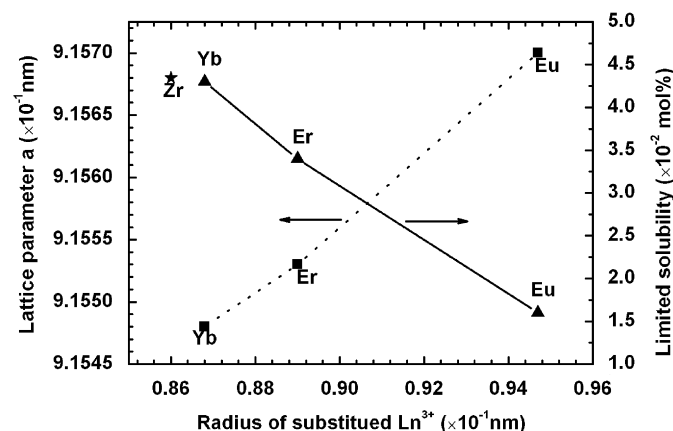


Fig. 8. Lattice parameters of saturated solid solutions and limited solubility of  $Zr_{1-x}Ln_xW_2O_{8-x/2}$  as a function of the radius of substituted  $Ln^{3+}$  ions. The inserted star represents pure  $ZrW_2O_8$  as the reference point.

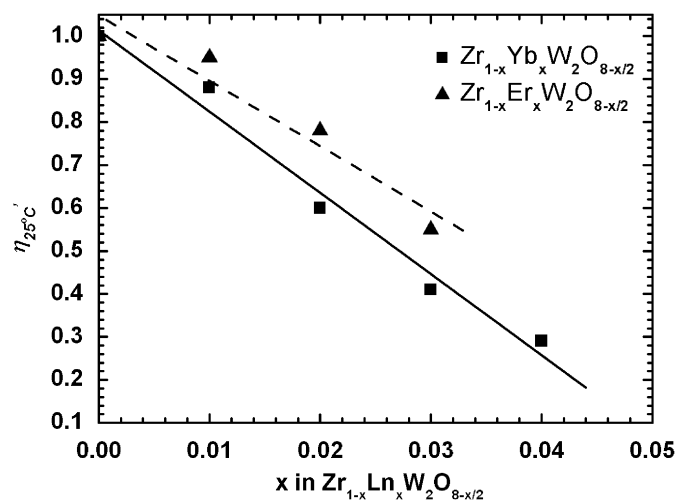


Fig. 9. Relative order parameter ( $\eta_{25^\circ C}$ ) against the concentration ( $x$ ) of  $Ln^{3+}$  in  $Zr_{1-x}Ln_xW_2O_{8-x/2}$ .

in both cases implies that variation of the phase transition temperature seems to be associated with the change in relative order degree of the solid solution induced by trivalence ion substitution, which leads to a decrease in the number of the orientationally ordered  $WO_4$  pairs [18]. By the same reasoning, the ionic radius-dependence of relative order parameters,  $\eta_{25^\circ C}$  of  $Zr_{1-x}Ln_xW_2O_{8-x/2}$  solid solutions would also be rationalized.

#### 4. Conclusion

$Zr_{1-x}Ln_xW_2O_{8-x/2}$  partial solid solutions with  $Ln = Yb$ ,  $Er$  and  $Eu$  have been synthesized. The XRD patterns of these solid solutions have been indexed based on the cubic  $\alpha$ - $ZrW_2O_8$  structural and their lattice parameters were found to be described by Vegard's rule. The CTE of these solid solutions was estimated to be  $-10.3 \times 10^{-6} K^{-1}$  in temperature range of 30–100 °C. The gradually change in CTE observed at temperature above 100 °C implies that a phase transformation occurs in a higher temperature region. The limited solubility of lanthanide ions in  $Zr_{1-x}Ln_xW_2O_{8-x/2}$  solid solutions at sintering temperature was found to decrease with an increase in their radius. Specifically; the limited solubility is estimated to be about 4.4, 3.3 and 1.6 mol% for  $Yb^{3+}$ ,  $Er^{3+}$  and  $Eu^{3+}$ , respectively. In the meantime, a novel method for evaluating limited solubility of lanthanide ions in  $Zr_{1-x}Ln_xW_2O_{8-x/2}$  solid solutions has been developed based on the  $x$ -dependence of the phase transition temperatures  $T_c$ .

#### Acknowledgments

Supports for this research from the National Science Foundation of China under Grant NSFC 20471010 and Foundation of Beijing Key Discipline of Inorganic Chemistry of Beijing Education Committee are gratefully acknowledged.

#### References

- [1] T.A. Mary, J.S.O. Evans, T. Vogt, A.W. Sleight, *Science* 272 (1996) 90–92.
- [2] J.S.O. Evans, T.A. Mary, T. Vogt, M.A. Subramanian, A.W. Sleight, *Chem. Mater.* 8 (1996) 2809–2823.
- [3] N. Duan, U. Kameswari, A.W. Sleight, *J. Am. Chem. Soc.* 121 (1999) 10432–10433.
- [4] J.S.O. Evans, *J. Chem. Dalton Trans.* (1999) 3317–3326.
- [5] X.B. Deng, X.H. Zhao, J.S. Han, *Chin. J. Inorg. Chem.* 21 (9) (2005) 1357–1362.
- [6] C. Lind, A.P. Wilkinson, Zh. Hu, S. Short, J.D. Jorgensen, *Chem. Mater.* 10 (1998) 2335–2337.
- [7] C. Lind, A.P. Wilkinson, C.J. Rawn, E.A. Payzant, *J. Mater. Chem.* 11 (2001) 3354–3359.
- [8] C. Cloosmann, A.W. Sleight, *J. Solid State Chem.* 139 (1998) 424–426.
- [9] Sh.Y. Zhang, X.H. Zhao, H. Ma, *Chin. J. Chem.* 18 (4) (2000) 571–575.
- [10] J.S.O. Evans, P.A. Hanson, R.M. Ibberson, *J. Am. Chem. Soc.* 122 (2000) 8694–8699.

- [11] L. Huang, Q.G. Xiao, H. Ma, G.B. Li, F.H. Liao, Ch.M. Qi, X.H. Zhao, *Eur. J. Inorg. Chem.* (2005) 4521–4526.
- [12] C.D. Meyer, F. Bouree, J.S.O. Evans, K. De Buysser, E. Bruneel, I.V. Driessche, S. Hoste, *J. Mater. Chem.* 14 (2004) 2983–2994.
- [13] N. Nakajima, Y. Yamamura, T. Tsuji, *Solid State Commun.* 128 (2003) 193–196.
- [14] Y. Yamamura, M. Kato, T. Tsuji, *Thermochim. Acta* 431 (2005) 24–28.
- [15] T.J.B. Holland, S.A.T. Redfern, *Mineral. Mag.* 61 (1997) 65–77.
- [16] L.Y. Luke, M.G. Chang, B. Scroger, J. Phillips, *Am. Ceram. Soc.* 42 (1967) 211–215.
- [17] C. Dong, *J. Appl. Crystallogr.* 32 (1999) 838.
- [18] Y. Yamamura, N. Nakajima, T. Tsuji, *Phys. Rev. B* 64 (2001) 184109.
- [19] E.J. Sonneveld, R. Delhez, Philips Electronics N. V., 1996.